Heat accumulation during pulsed laser materials processing

Rudolf Weber,* Thomas Graf, Peter Berger, Volkher Onuseit, Margit Wiedenmann, Christian Freitag, and Anne Feuer

IFSW, University of Stuttgart, Pfaffenwaldring 43, D-70569 Stuttgart, Germany
**rudolf.weber@ifsw.uni-stuttgart.de*

Abstract: Laser materials processing with ultra-short pulses allows very precise and high quality results with a minimum extent of the thermally affected zone. However, with increasing average laser power and repetition rates the so-called heat accumulation effect becomes a considerable issue. The following discussion presents a comprehensive analytical treatment of multi-pulse processing and reveals the basic mechanisms of heat accumulation and its consequence for the resulting processing quality. The theoretical findings can explain the experimental results achieved when drilling microholes in CrNi-steel and for cutting of CFRP. As a consequence of the presented considerations, an estimate for the maximum applicable average power for ultra-shorts pulsed laser materials processing for a given pulse repetition rate is derived.

OCIS codes: (140.3390) Laser materials processing; (140.6810) Thermal effects.

References and links

1. J.-P. Negel, A. Voss, M. Abdou Ahmed, D. Bauer, D. Sutter, A. Killi, and T. Graf, "1.1 kW average output power from a thin-disk multipass amplifier for ultrashort laser pulses," Opt. Lett. **38**(24), 5442–5445 (2013).
2. H. Hügel, H. Schittenhelm, K. Jasper, G. Callies, and P. Berger, "Structuring with excimer lasers - experimental and theoretical investigations on quality and efficiency," J. Laser Appl. **10**(6), 255–264 (1998).
3. W. Schulz, U. Eppelt, and R. Poprawe, "Review on laser drilling I. Fundamentals, modeling, and simulation," J. Laser Appl. **25**(1), 012006 (2013).
4. S. Nolte, C. Momma, H. Jacobs, A. Tünnermann, B. N. Chichkov, B. Wellegehausen, and H. Welling, "Ablation of metals by ultrashort laser pulses," J. Opt. Soc. Am. B **14**(10), 2716–2722 (1997).
5. D. Hellrung, A. Gillner, and R. Poprawe, "Laser beam removal of micro-structures with Nd: YAG lasers," Proc. Lasers Mater. Processing Laser **97**, 267–273 (1997).
6. T. V. Kononenko, V. I. Konov, S. V. Garnov, R. Danielius, A. Piskarskas, G. Tamosauskas, and F. Dausinger, "Comparative study of the ablation of materials by femtosecond and pico- or nanosecond laser pulses," Quantum Electron. **29**(8), 724–728 (1999).
7. R. Weber, A. Michalowski, M. Abdou-Ahmed, V. Onuseit, V. Rominger, M. Kraus, and T. Graf, "Effects of radial and tangential polarization in laser material processing," Phys. Procedia **12**, 21–30 (2011).
8. R. Weber, M. Hafner, A. Michalowksi, and T. Graf, "Minimum damage in CFRP laser processing," Phys. Procedia **12**(2), 302–307 (2011).
9. B. Neuenschwander, B. Jaeggi, M. Schmid, U. Hunziker, B. Luescher, and C. Nocera, "Processing of industrially relevant non-metals with laser pulses in the range between 10ps and 50ps," in *Proceedings of the International Congress on Applications of Lasers & Electro-Optics (ICALEO)*, Paper M (**Vol. 103**) (2011).
10. M. Kraus, C. Markmann, A. Michalowski, R. Weber, and T. Graf, "Gas-assisted microdrilling in steel with ultrashort pulsed laser radiation," in *LPM2010*, Stuttgart, June 7- June 10 (2010).
11. A. Ancona, S. Döring, C. Jauregui, F. Röser, J. Limpert, S. Nolte, and A. Tünnermann, "Femtosecond and picosecond laser drilling of metals at high repetition rates and average powers," Opt. Lett. **34**(21), 3304–3306 (2009).
12. S. Eaton, H. Zhang, P. Herman, F. Yoshino, L. Shah, J. Bovatsek, and A. Arai, "Heat accumulation effects in femtosecond laser-written waveguides with variable repetition rate," Opt. Express **13**(12), 4708–4716 (2005).
13. R. R. Gattass, L. R. Cerami, and E. Mazur, "Micromachining of bulk glass with bursts of femtosecond laser pulses at variable repetition rates," Opt. Express **14**(12), 5279–5284 (2006).
14. R. Weber, V. Onuseit, S. Tscheulin, and T. Graf, "High-efficiency laser processing of CFRP," in *Proc. ICALEO 2013* (2013), Paper LMP 1901.

#207073 - $15.00 USD Received 24 Feb 2014; revised 29 Mar 2014; accepted 31 Mar 2014; published 2 May 2014

15. T. Tamaki, W. Watanabe, and K. Itoh, "Laser micro-welding of transparent materials by a localized heat accumulation effect using a femtosecond fiber laser at 1558 nm," Opt. Express **14**(22), 10460–10468 (2006).
16. A. A. Cenna and P. Mathew, "Evaluation of cut quality of fibre-reinforced plastic – a review," Int. J. Mach. Tools Manuf. **37**(6), 723–736 (1997).
17. D. Herzog, P. Jaeschke, O. Meier, and H. Haferkamp, "Investigations on the thermal effect caused by laser cutting with respect to static strength of CFRP," Int. J. Mach. Tools Manuf. **48**(12-13), 1464–1473 (2008).
18. A. Goeke and C. Emmelmann, "Influence of laser cutting parameters on CFRP part quality," Phys. Procedia **5**, 253–258 (2010).
19. A. Klotzbach, M. Hauser, and E. Beyer, "Laser cutting of carbon fibre reinforced polymers using highly brilliant laser beam sources," Phys. Procedia. **12**, 572–577 (2011).
20. R. Weber, M. Hafner, A. Michalowski, P. Mucha, and T. Graf, "Analysis of thermal damage in laser processing of CFRP," in *Proc. ICALEO 2011* (2011).
21. R. Weber, C. Freitag, T. Kononenko, M. Hafner, V. Onuseit, P. Berger, and T. Graf, "Short-pulse laser processing of CFRP," Phys. Procedia **39**, 137–146 (2012).
22. H. Deutsche Edelstahlwerke Gmb, Werkstoffdatenblatt 1.4301_de.pdf, http://www.dew-stahl.com/fileadmin/files/dew-stahl.com/documents/Publikationen/Werkstoffdatenblaetter/RSH/1.4301_de.pdf.
23. D. E. Kline, "Thermal Conductivity Studies of Polymers," J. Polym. Sci., Polym. Phys. Ed. **1**, 441–450 (1961).
24. S. D. McIvor, M. I. Darby, G. H. Wostenholm, B. Yates, L. Banfield, R. King, and A. Webb, "Thermal conductivity measurements of some glass fibre- and carbon fibre-reinforced plastics," J. Mater. Sci. **25**(7), 3127–3132 (1990).
25. P. Morgan, *Carbon Fibers and Their Composites* (CRC Press, 2005), p. 121.
26. M. W. Pilling, B. Yates, M. A. Black, and P. Tattersall, "The thermal conductivity of carbon fibre-reinforced composites," J. Mater. Sci. **14**(6), 1326–1338 (1979).
27. C. Pradere, J. C. Batsale, J. M. Goyhénèche, R. Pailler, and S. Dilhaire, "Thermal properties of carbon fibers at very high temperature," Carbon **47**(3), 737–743 (2009).
28. R. Rolfes and U. Hammerschmidt, "Transverse thermal conductivity of CFRP laminates; a numerical and experimental validation of approximation formulae," Compos. Sci. Technol. **54**(1), 45–54 (1995).
29. F. R. Barnet and M. K. Norr, "A three-dimensional structural model for a high modulus pan-based carbon fibres," Composites **7**(2), 93–99 (1976).
30. N. N. Rykalin, *Die Wärmegrundlagen des Schweißvorgangs* (VEB Verlag Technik, 1957).
31. D. Radaj, *Heat Effects of Welding, Temperature Field, Residual Stress, Distortion* (Springer, 1992).
32. M. Hafner, R. Weber, and T. Graf, "Modeling of laser ablation of CFRP - influence of beam profile," Stuttgarter Lasertage SLT 12, Neue Messe Stuttgart (2012).
33. C. Freitag, R. Weber, and T. Graf, "Polarization dependence of laser interaction with carbon fibers and CFRP," Opt. Express **22**(2), 1474–1479 (2014).
34. T. Graf, R. Weber, V. Onuseit, M. Hafner, C. Freitag, and A. Feuer, "Laser applications from production to machining of composite materials," in *EALA 2012* (2012).

1. Introduction

The average power of commercial ultrafast lasers with almost diffraction limited beam quality is currently ranging in the order of few tens of Watts. Kilowatt systems with millijoule pulse energies are however already demonstrated [1] and precise laser materials processing such as micro drilling, surface structuring or micro-cutting continuously gains of importance for industrial applications. Lasers with short and ultra-short pulses, i.e. with pulse durations in the order of nanoseconds or pico- and femtoseconds, respectively, allow very precise high-quality processing of a wide range of materials [2–8]. The high processing quality is attributed to the fact that most of the absorbed energy is used for the ablation process. Therefore the surrounding material is left at comparably low temperatures - at least for single-pulse processes at low repetition rates.

Nevertheless the total absorbed incident laser pulse energy, $\eta_{Abs} \cdot E_{Pulse}$, where E_{Pulse} is the energy of the incident laser pulse and η_{Abs} the absorptance at the interaction zone, will always exceed the energy required for the mere material ablation process. For the case of material removal by sole evaporation (i.e. with neglectable melt expulsion) the ablation energy is given by the evaporated volume V_{Evap} times the total volume specific enthalpy h_{Evap} which is required for evaporation. The enthalpy h_{Evap} includes the heating of the material and its phase transitions. The difference $\eta_{Abs} \cdot E_{Pulse} - V_{Evap} \cdot h_{Evap}$ partly overheats the expanding vapor beyond the required evaporation temperature (by an amount of energy Q_{Vapor}) and partly is left as thermal energy Q_{heat} in the surrounding material that is not ablated. In the following Q_{heat} is referred to as residual heat. With this the energy balance reads

#207073 - $15.00 USD Received 24 Feb 2014; revised 29 Mar 2014; accepted 31 Mar 2014; published 2 May 2014

$$\eta_{Abs} \cdot E_{Pulse} = V_{Evap} \cdot h_{Evap} + Q_{Vapor} + Q_{Heat} \quad (1)$$

Defining the thermal efficiency by $\eta_{th} = \left(V_{Evap} h_{Evap} + Q_{Vapor}\right) / \eta_{Abs} E_{Pulse}$ and the fraction $\eta_{Heat} = Q_{Heat} / E_{Pulse}$ the residual heat is then given by

$$Q_{Heat} = \eta_{Abs} \cdot (1 - \eta_{Th}) \cdot E_{Pulse} = \eta_{Heat} \cdot E_{Pulse} \quad (2)$$

It is noted that η_{Th}, η_{Abs}, and hence η_{Heat} are usually complicated, time-dependent functions of processing parameters such as material properties, actual geometry of the interaction zone and the workpiece and in particular also of the incident fluence and the ablation threshold [9] which will qualitatively be discussed later in this paper. However, to facilitate the understanding of heat accumulation, η_{Heat} is assumed to be constant for the following. Typically the residual heat generated during the ablation processes by a single ultra-short laser pulse is comparably small and avoids detrimental effects on the workpiece. With increasing repetition rate, however, the residual heat may not be removed fast enough by heat conduction into the workpiece which leads to a significant impact on the achievable process quality. Figure 1 shows helically drilled holes in CrNi-steel giving a typical example of the thermal influence on materials processing with a repetitively pulsed laser [10]. The upper row shows the drilling inlet (i.e. the side from which the laser processing takes place), the lower row the outlet. The respective laser parameters are noted below each pair of pictures.

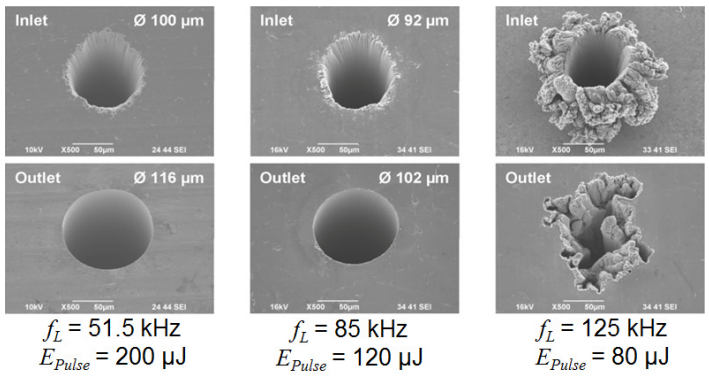

Fig. 1. SEM pictures of helically drilled holes in 1 mm thick CrNi-steel plates [10]. The upper pictures show the inlet, the lower the outlet of the drilling. The holes were drilled at the same average power of 10.3 W with a pulse duration of 6 ps and a focal spot diameter of 25 µm. The respective repetition rates (f_L) and pulse energies (E_p) used for the drilling process are noted below each pair of pictures.

The average laser power of 10.3 W was the same for all three boreholes. Nevertheless it is clearly seen, that the increase of the pulse repetition rate, f_L, (from left to right) has a dramatic influence on the achieved processing quality although the laser fluence was about 40 times above ablation threshold. The reason for this behavior is usually referred to as "heat accumulation" which is often observed in pulsed laser processing [11,12] and sometimes even utilized for materials processing [13–15]. However, with increasing average power this effect is more and more difficult to control and can be the dominant effect for material damage in the surrounding of the processed area. Due to the special material properties this is particularly pronounced in processing of carbon fiber reinforced plastics (CFRP) [16–21].

A comprehensive analytical treatment of the thermal effects during repetitively pulsed laser processing as presented in the following is therefore important to understand the associated quality issues. It allows predicting the influence of the various parameters of multi-pulse processing and gives a consistent definition of heat accumulation. The calculations are compared to experimental data achieved in CrNi-steel and CFRP. As material data differ from

#207073 - $15.00 USD Received 24 Feb 2014; revised 29 Mar 2014; accepted 31 Mar 2014; published 2 May 2014

different sources [22–28] averaged material data were used for the calculations throughout the whole paper. The significantly higher thermal diffusivity parallel to the carbon fiber axis results from the internal structure of the fibers (i.e. onion skin type, graphite-like layers along the axis in the outer region of the fibers [29]). The values are summarized in Table 1.

Table 1. Material values used for the calculations in this paper.

Material	Thermal diffusivity in 10^{-5} m^2/s	Density in kg/m^3	Heat capacity in J/kgK	Melting temperature in °C	Evaporation temperature in °C
CrNi-steel	0.40	7900	477	1500	3000
Carbon fibers parallel to axis	3.81	1850	710	-	3600
perpendicular	0.38	1850	710	-	3600
Plastic matrix	0.01	1250	1200	-	800

2. Temperature fields induced by a single pulse

In the late fifties N.N. Rykalin introduced solutions of the heat conduction equation to describe the laser welding process [30] in semi-infinite and infinite bodies, conveniently summarized in [31]. The same solutions are very useful to investigate the temporal and spatial evolution of the temperature field caused by short-pulse laser processing. In [30] the solutions were deduced for the three heat source geometries plane surface (one-dimensional (1D) heat conduction), line (two-dimensional (2D) heat conduction) and point source (three-dimensional (3D) heat conduction) shown in a slightly modified version of the original pictures in Figs. 2(a)–2(c). In isotropic materials the choice of these source geometries is motivated by the dimensional reduction of the heat conduction from three-dimensional in the case of the point source to two-dimensional in the case of the line source and one-dimensional in the case of the plane source. To some extent the solutions may also be applied when the dimensionality of the heat flow is confined by anisotropic material properties or geometries.

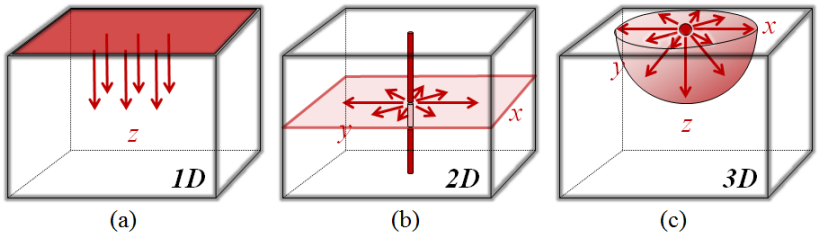

Fig. 2. Geometry of the heat source and the dimension of the resulting temperature fields.

The solution of the 1D heat flow can e.g. be applied to long, thin fibers with no radial heat exchange with its surrounding. In addition, the heat flow may be approximated as 1D during the heating phase of a pulse on a plane surface when the thermal diffusion length is much smaller than the radius of the incident laser beam. After a comparably long time, i.e. when the diffusion length has become larger than the radius of the laser beam on the surface, the resulting temperature field in homogeneous materials is dominated by a 3D heat flow. The 2D case is useful to describe elongated heat sources such as deep capillaries during deep penetration welding. In addition it can be applied for materials with defined, heat conducting layers, such as thin sheets or laminated materials.

Solving the heat conduction equation for the 1D, 2D and 3D heat flow, respectively, leads to the temperature fields [30]

#207073 - $15.00 USD Received 24 Feb 2014; revised 29 Mar 2014; accepted 31 Mar 2014; published 2 May 2014

$$\textbf{1D} \qquad T_{1D} - T_0 = \Delta T_{1D} = \frac{Q_{1D}}{r \cdot c_p \cdot \sqrt{4 \cdot p \cdot k \cdot t}} e^{-\frac{r^2}{4 \cdot k \cdot t}} \qquad \left(r^2 = z^2\right) \qquad (3a)$$

$$\textbf{2D} \qquad T_{2D} - T_0 = \Delta T_{2D} = \frac{Q_{2D}}{r \cdot c_p \cdot \sqrt{\left(4 \cdot p \cdot k \cdot t\right)^2}} e^{-\frac{r^2}{4 \cdot k \cdot t}} \qquad \left(r^2 = x^2 + y^2\right) \qquad (3b)$$

$$\textbf{3D} \qquad T_{3D} - T_0 = \Delta T_{3D} = \frac{Q_{3D}}{r \cdot c_p \cdot \sqrt{\left(4 \cdot p \cdot k \cdot t\right)^3}} e^{-\frac{r^2}{4 \cdot k \cdot t}} \qquad \left(r^2 = x^2 + y^2 + z^2\right) \qquad (3c)$$

where ΔT_{nD} is the temperature increase with respect to the initial temperature T_0, $nD \in [1,2,3]$, ρ is the mass density of the solid or liquid material, c_p its specific heat capacity, $\kappa = \lambda_{th} / (\rho\, c_p)$ the temperature conductivity, λ_{th} the heat conductivity, t is time, and x,y,z are the spatial coordinates. As a simplification, the material properties ρ, c_p, and λ_{th} are assumed to be constant with respect to temperature. Typically $T_0 \approx 0°C$ allowing to compare temperature increases e.g. with absolute phase transition temperatures in the following.

The process quality is governed by the residual heat Q_{heat} left in the workpiece and the corresponding temperature distributions reached therein. In this context the heat inputs Q_{nD}, are determined by the residual energy as defined in Eq. (2). The heat sources Q_{1D} *[energy per unit area],* Q_{2D} *[energy per unit length],* and Q_{3D} *[energy]* define the heat which is released in an infinitely short time at $t = 0$. Actually Q_{1D} is a plane source, Q_{2D} a line source and Q_{3D} a point source, but to ease the notation in the following, these sources are labeled with the dimensionality of the corresponding heat flow. Explicitly, the heat sources read

$$\textbf{1D} \qquad Q_{1D} = 2 \cdot Q_{Heat} / A \qquad \left(\text{in J/m}^2\right) \qquad (4a)$$

$$\textbf{2D} \qquad Q_{2D} = Q_{Heat} / \ell \qquad \left(\text{in J/m}\right) \qquad (4b)$$

$$\textbf{3D} \qquad Q_{3D} = 2 \cdot Q_{Heat} \qquad \left(\text{in J}\right) \qquad (4c)$$

where A and ℓ are the area and the length of the interaction zone, respectively. The factor of two in the numerator of the 1D and the 3D case has to be introduced when the heat source is located on a surface allowing heat flow only into one half space.

It is important to note that this thermal input energy is applied instantaneously (at $t = 0$), i.e. the heating phase is not considered with this formalism: At this instance of time Eqs. (3a)–(3c) always yield an unphysical infinite temperature [30].

In the analytical solutions given in Eqs. (3a) and (3b), the heat sources formally correspond to an infinite large plane and an infinitely long line, respectively. As this does not apply for real situations with finite extensions of the heat sources, care has to be taken to correctly define the values Q_{1D} and Q_{2D} and to consider the analytical solutions only in the domains which are consistent with the underlying assumptions of 1D or 2D heat flow as discussed above.

A comparison of the three Eqs. (3a)–(3c) reveals that for each additional dimension which can contribute to the heat flow the equation is multiplied by $1/\sqrt{\left(4\pi\kappa t\right)}$ and the coordinate of space, r, is extended by one coordinate axis. Hence Eqs. (3a)–(3c) can be written in the convenient, generalized form

$$nDim \qquad T_{nD} - T_0 = \Delta T_{nD} = \frac{Q_{nD}}{r \cdot c_p \cdot \sqrt{\left(4 \cdot p \cdot k \cdot t\right)^{nD}}} e^{-\frac{1}{t}\frac{r_{nD}^2}{4 \cdot k}} \qquad (5)$$

#207073 - $15.00 USD Received 24 Feb 2014; revised 29 Mar 2014; accepted 31 Mar 2014; published 2 May 2014

As an example Fig. 3 shows the calculated temperature evolution ΔT_{3D} in CrNi-steel as a function of time for Q_{3D} = 0.1 µJ and Q_{3D} = 1 µJ of residual heat deposited on the surface at $x = y = z = 0$ (a) and as a function of space for different times after 1 µJ of heat input on the surface at $x = y = z = 0$ (b).

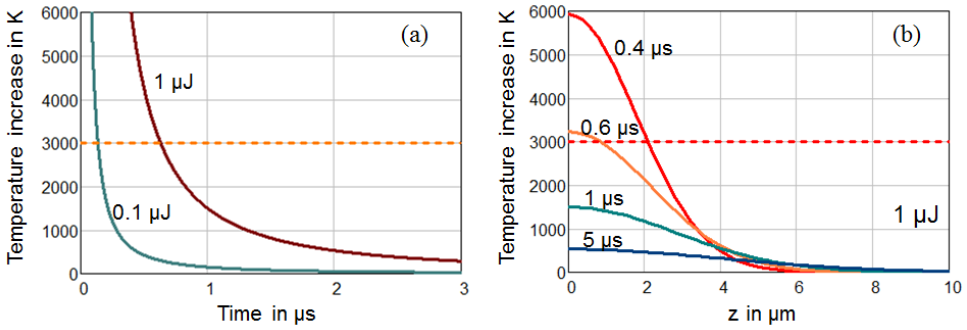

Fig. 3. Temperature increase ΔT_{3D} as a function of time for 0.1 µJ and 1 µJ of heat input in steel at the position of the heat source (left) and as a function of space for different instances of time after the heat deposition (right). The dashed lines indicate the evaporation temperature of CrNi-steel.

From Fig. 3(a) one can also identify the unphysical high temperature on the surface for very short times due to the infinitesimally small point source and the infinitesimally short duration of the energy input assumed in the model [30]. Despite this singularity the main conclusion is that the temperature increase is much higher for the larger input energy. After a time period which depends on the thermal input energy the surface temperature drops below evaporation temperature (shown by the dashed line). This marks the begin of the validity of the model. In the example shown in Fig. 3(b) this occurs about 0.6 µs after the thermal energy was deposited. After this time the temperature distribution as a function of space also shows the well-known Gaussian shape. One can also note that the width of the temperature distribution (i.e. the thermal diffusion length) is in the order of the radius of a typical short-pulse laser processing focus which requires the use of the 3D solution (rather than the 1D solution which is only valid as long as the diffusion length is much smaller than focal spot radius).

3. Multi-pulse temperature fields

The above equations describe the heat input and the resulting temperature distribution caused by a single (infinitely short) laser pulse. In order to consider the effect of a series of pulses delivered with a repetition rate f_L, Eq. (5) can be extended in the form

$$\Delta T_{nD}(t,N) = \frac{Q_{nD}\cdot\Theta\left(t-\frac{N-1}{f_L}\right)}{r\cdot c_p\cdot\sqrt{\left(4\cdot p\cdot k\cdot\left(t-\frac{N-1}{f_L}\right)\right)^{nD}}}\, e^{-\frac{1}{\left(t-\frac{N-1}{f_L}\right)}\frac{r_{nD}^2}{4\cdot k}} \tag{6}$$

to denote the contribution to the temperature increase by the *N-th* pulse which is incident at a time delay of $(N-1)/f_L$ after the first pulse at $t = 0$. The Heaviside function Θ is equal to zero for arguments <0 and equal to one for arguments ≥0.

The spatial-temporal temperature contributions of multiple heat sources can be summed up as long as the material properties can be considered as constant with temperature, as already assumed for the set of Eqs. (3a)–(3c). Hence, the superposition of the temperature

#207073 - $15.00 USD Received 24 Feb 2014; revised 29 Mar 2014; accepted 31 Mar 2014; published 2 May 2014

fields of a number of N_P pulses is given by the sum over the contribution given in Eq. (6) of the individual pulses

$$\Delta T_{Sum,nD}(t) = \sum_{N=1}^{N_P} \Delta T_{nD}(t,N) \tag{7}$$

where $N_P = floor(t_{IntAct} \cdot f_L) + 1$ is the number of pulses which are incident at the interaction zone with the repetition rate f_L during the interaction time, $t_{IntActroc}$. The function *floor(x)* yields the largest integer which is smaller or equal to the real argument x.

Inserting Eq. (6) into Eq. (7) one finds

$$\Delta T_{Sum,nD}(t) = \frac{Q_{nD}}{\rho \cdot c_p \cdot \sqrt{(4 \cdot \pi \cdot \kappa)^{nD}}} \sum_{N=1}^{N_P} \frac{\Theta\left(t - \frac{N-1}{f_L}\right)}{\sqrt{\left(t - \frac{N-1}{f_L}\right)^{nD}}} e^{-\frac{1}{\left(t-\frac{N-1}{f_L}\right)} \cdot \frac{r_{nD}^2}{4 \cdot \kappa}} \tag{8}$$

as the explicit expression for the temporal evolution of the temperature increase caused by a series of N_p pules, delivered at a repetition rate f_L.

The resulting 3D temperature increase, $\Delta T_{Sum,3D}$, on the surface at the location (i.e. $x = y = z = 0$ mm) of the released heat energy is shown for different examples in Fig. 4. To demonstrate the effect of repetitive pulses with $Q_{3D} = 5$ µJ Fig. 4(a) shows the temperature evolution for the two different repetition rates $f_L = 50$ kHz and $f_L = 250$ kHz, again calculated for CrNi-steel.

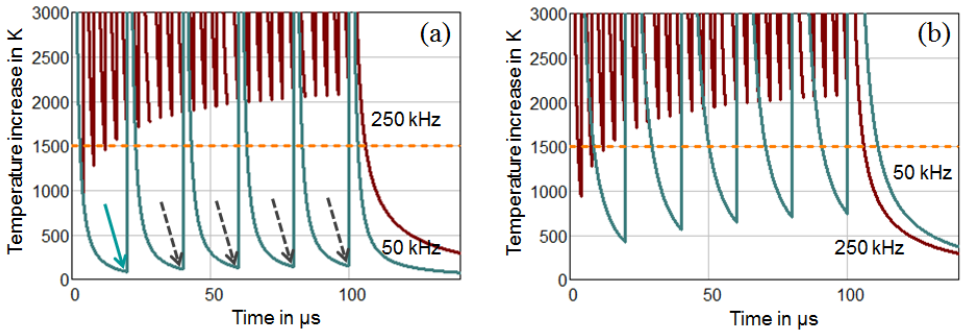

Fig. 4. Temporal evolution of the temperature increase $\Delta T_{Sum,3D}$ on the surface of a semi-infinite body of CrNi-steel at the location of a point source for two different repetition rates and the same heat source energy of 5 µJ per pulse (a) or the same average power of 1.25 W, i.e. with a pulse energy of 25 µJ at 50 kHz and 5 µJ at 250 kHz (b).

Note that according to the assumptions of the model explained above, only the residual heat which is not removed with the ablated material is considered here. Hence the ablation process itself is not considered and the validity of the calculated temperatures [30] is restricted to the values of at least below evaporation temperature which is about 3000°C for CrNi-steel. This is why the diagrams in Fig. 4 are truncated at 3000 K.

Following the curve for $f_L = 50$ kHz in Fig. 4(a), the surface temperature after the first pulse cools down to a residual increase of about 100 K after 20 µs before the second pulse hits the same spot (solid green arrow). With every subsequent pulse the surface is heated again in the same manner as after the first pulse but starting at a different, slightly increased offset temperature (dashed black arrows). In the following we refer to this increased offset temperature as the effect of heat accumulation.

The red curve in Fig. 4(a) shows the effect of an increased repetition rate of 250 kHz while keeping the input pulse energy constant at 5 µJ. The second pulse is released already after 5 µs when the surface is not yet significantly cooled down. This continues with the

#207073 - $15.00 USD Received 24 Feb 2014; revised 29 Mar 2014; accepted 31 Mar 2014; published 2 May 2014

subsequent pulses which yields a much higher heat accumulation than for the lower repetition rate of 50 kHz.

The quality of ablating laser processes is mainly determined by the temperatures reached in the non-ablated material next to the interaction zone. In Fig. 4 the dashed line represents the melting temperature of steel as a characteristic critical temperature that should not be exceeded to avoid quality issues. If the heat accumulation leads to a temperature increase exceeding this melting temperature, the surface of the material remains liquid between two subsequent pulses and each new pulse hits a still liquid surface which leads to a completely different and in particular no longer "cold" process and which will be dominated by hydrodynamic effects.

In the examples of Fig. 4 the laser is switched off after an interaction time of 100 µs. The cooling phase after the end of the laser interaction is of particular interest in the case of multipass laser processing.

The examples discussed so far in Fig. 4(a) are characterized by the same heating energy per pulse which means that the two curves correspond to two different average powers. An important aspect is found when comparing different repetition rates with the same average heating power as shown in Fig. 4(b). Although the average power is kept constant at 1.25 W (i.e. with a pulse energy of 25 µJ at 50 kHz and 5 µJ at 250 kHz) the heat accumulation is significantly larger with the higher repetition rate. This result is not a priori obvious but very important for a proper process design. Interestingly the cooling after the last pulse is faster for the lower pulse energy at the higher repetition rate which might be another critical aspect especially for applications with multipass processes.

It is noted that each single pulse creates very high temperatures leading to thermal effects in the surrounding materials. The damage caused by single pulses in CFRP was treated extensively e.g. in [8]. The scope of this paper is the heat accumulation effect due to multiple pulses onto the same spot.

4. Maximum reach of a given temperature

The processing quality is usually determined simply by the extent of material damage or – depending on material and purpose of the process – by the thickness of an occurring liquid layer. Knowing the critical temperature increase ΔT (e.g. to the melting temperature in the case of steel or to the matrix damage temperature in the case of CFRP) this damaging extent results from Eq. (7) by solving for the respective coordinate. The maximum reach of a given critical temperature is then found by differentiating with respect to time and setting the result to zero. As the coordinate giving the extent of the critical temperature is part of the function in the exponent inside the sum this can only be solved numerically and is beyond the scope of this paper. An example for such a solution was given in [8,21] for a 2D calculation of the extent of the matrix damage in CFRP.

5. Discussion of the thermal efficiency and the portion of the residual heat

The thermal efficiency η_{Th} defines the fraction of the incident pulse energy being converted to the thermal energy required for the process. As discussed in the introduction the remaining heat is left in the workpiece and its amount $Q_{Heat} = \eta_{Heat} \cdot E_{Pulse}$ is given in Eq. (2). Due to the volume specific enthalpy required for the evaporation of each material and the material optical properties this fraction η_{Heat} depends on the material properties, the pulse energy, the pulse duration, the beam intensity distribution and the fluence above threshold, as partly discussed in [9,32].

Furthermore, η_{Heat} is usually even changing with time during processing of the material. One reason is that depth and shape of the structure which is created during the process changes with the number of pulses – and hence with time – modifying the absorbed fluence due to scattering on the structure walls, the changing angle of incidence, and the changing total area of the interacting surface. As η_{Heat} is additionally affected by the material-dependent

#207073 - $15.00 USD Received 24 Feb 2014; revised 29 Mar 2014; accepted 31 Mar 2014; published 2 May 2014

absorptivity (see Eq. (2)) this leads to temporal variations of Q_{Heat} during the process in anisotropic materials.

In the end the fraction η_{Heat} of the incident energy converted to the residual heat Q_{Heat} is even a function of the heat accumulation itself, as material properties and surface structures also depend on the temperature. The determination of the correct amount of the residual energy Q_{Heat} is therefore a complex topic and is subject of further investigations.

In order to gain a basic understanding of the heat accumulation effect with the present state of knowledge and for the sake of simplicity each of the following examples was calculated with an adapted, constant fraction η_{Heat}. Despite this quite constricting assumption the experimental results are explained with very good agreement confirming that the basic understanding of heat accumulation is not significantly compromised by this simplification.

6. Solution for the temperature increase caused by heat accumulation

The temperature offset, i.e. the temperature increase caused by heat accumulation, after N_P pulses at the origin of the heat source at the time just before the subsequent pulse is regarded as suitable indicator to assess the processing quality.

At the location $x = y = z = 0$, where the exponential function in Eq. (8) equals 1, this temperature offset immediately before each individual pulse is given by evaluating Eq. (8) at the times $t = (N_t\text{-}\delta)/f_L$, which yields

$$\Delta T_{HA,nD}\left(t=\frac{N_t-\delta}{f_L}\right)=\frac{Q_{nD}}{\rho\cdot c_p\cdot\sqrt{\left(\frac{4\cdot\pi\cdot\kappa}{f_L}\right)^{nD}}}\sum_{N=1}^{N_p}\frac{\Theta\left(N_t-\delta-N+1\right)}{\sqrt{\left(N_t-\delta-N+1\right)^{nD}}} \tag{9}$$

where N_t is an integer and δ/f_L is an infinitesimally small time. This expression (with $\delta\to 0$) actually describes the lower envelope of Eq. (8) and of the curves shown in Fig. 4.

From this and our definition of heat accumulation as given in Fig. 4(a) the temperature offset caused after the series of the N_p pulses is then found at the time given by $N_t = N_p$ which (for $\delta\to 0$) leads to

$$\Delta T_{HA,nD}\left(t=\frac{N_p}{f_L}\right)=\frac{Q_{nD}}{\rho\cdot c_p\cdot\sqrt{\left(\frac{4\cdot\pi\cdot\kappa}{f_L}\right)^{nD}}}\sum_{N=1}^{N_p}\frac{1}{\sqrt{N^{nD}}} \tag{10}$$

which is called heat accumulation equation in the following.

7. Comparison with experimental results

The validity of the above theoretical considerations was examined by comparing the calculations with experimental results for laser processing of an isotropic and an anisotropic material which can be described by 3D and 1D heat flow, respectively.

7.1 Heat accumulation for 3D heat flow in CrNi-steel

Figure 5 shows the calculated heat accumulation resulting during laser processing of CrNi-steel with the parameters used to helically drill the holes shown in Fig. 1. The fraction η_{Heat} was the only free (fitting) parameter and was set to be 12.5% for all three drilling parameters in order to correctly describe the experimental results. As mentioned above the average power is the same for all three processes.

#207073 - $15.00 USD Received 24 Feb 2014; revised 29 Mar 2014; accepted 31 Mar 2014; published 2 May 2014

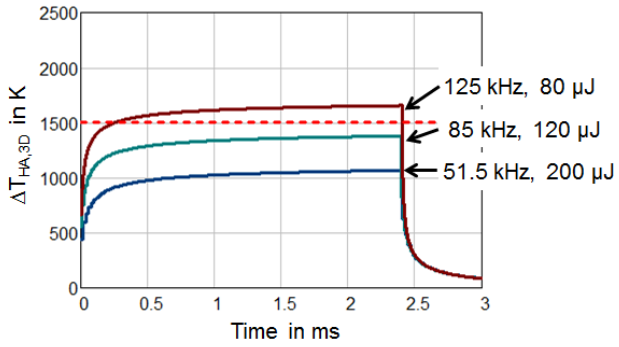

Fig. 5. Calculated temperature increase, $\Delta T_{HA,3D}$, caused by heat accumulation in CrNi-steel for the three laser parameters used to drill the holes shown in Fig. 1. The dashed line is the melting temperature of steel.

The focus diameter was d_{Beam} = 20 µm. With the helical drilling radius of 40 µm and the used helical revolution speed of 2000 rpm this yields a feed rate of v = 8.4 mm/s. The local interaction time $t_{IntAct} = d_F / v$ used in the calculation therefore amounts to 2.4 ms.

It can be seen, that the temperature increase caused by the heat accumulation during processing with a repetition rate of 51.5 kHz remain well below the melting temperature of steel. With a repetition rate of 85 kHz (and correspondingly lower pulse energy to keep the average power constant) the temperature increase reached by the heat accumulation is still below but already close to melting temperature which might manifest itself in additional structures in the hole inlet as seen in the middle top picture of Fig. 1. At the higher repetition rate of 125 kHz the accumulated temperature increase significantly exceeds the melting temperature of steel already after less than 0.5 ms. This means that the whole drilling process occurs with a molten material surface and results in an unacceptable quality of the holes as seen in the right pictures of Fig. 1.

The time interval between two consecutive passes of the beam during the helical drilling process is almost 30 ms. The calculations also show that the heating effect of subsequent passes of the beam is negligible as the workpiece surface is efficiently cooled down within this time (see the temperature curves in Fig. 5 for t > 2.4 ms for comparison).

7.2 Heat accumulation for 1D heat flow in CFRP

CFRP is used as an example for 1D heat flow in the following. Figure 6 shows a sketch of the scaled top-view of the processed CFRP surface in order to describe the 1D heat flow characteristics and the fraction of pulse energy which is coupled into a single fiber. The laser beam was focused to a focal spot diameter of d_{Beam} = 15 µm onto the CFRP surface containing fibers with a (typical) diameters of d_{Fiber} = 5 µm with 50% of fill factor.

The laser beam is moved along the cutting direction. The largest possible interacting area of the focal spot with a single fiber is approximated as hatched rectangle in Fig. 6. The part of the pulse energy in this area creates a residual heat of $Q_{Heat} \approx \eta_{Heat} \cdot E_{Pulse} \cdot d_{Fibre} / d_{Beam}$ which is provided to each single fibre assuming a flat-top intensity profile and 100% absorption, i.e. neglecting correct coupling conditions as described in [33].

#207073 - $15.00 USD Received 24 Feb 2014; revised 29 Mar 2014; accepted 31 Mar 2014; published 2 May 2014

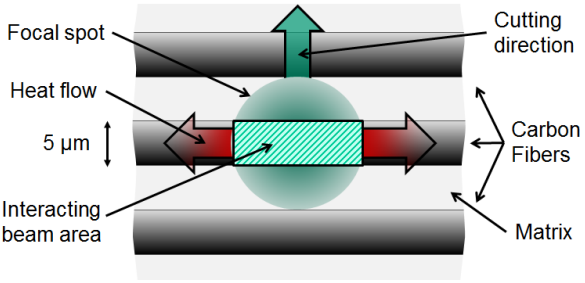

Fig. 6. Sketch of the 1D heat flow along the fibers during cutting of CFRP.

Considering the geometry and the material properties given in Table 1 it is assumed that the heat flow in CFRP occurs mainly along the individual fibers (i.e. perpendicular to the incoming laser beam) corresponding to a predominantly 1D heat flow as indicated by the arrows along the fiber in the center in Fig. 6. As the heat flows in both directions, to the left and to the right, only 50% of Q_{Heat} have to be considered for the calculation. This residual heat has to flow along one single fiber, i.e. through the cross-sectional area of one fiber, $A_{Fiber} = \pi \cdot (d_{Fiber} / 2)^2$. The 1D heat source as defined in Eq. (4a) is therefore given by $Q_{1D} = 0.5 \cdot Q_{Heat} / A_{Fibre} = 2 \cdot \eta_{Heat} \cdot E_{Pulse} \cdot / (\pi \cdot d_{Fibre} \cdot d_{Beam})$.

The pulse energy of 28 µJ as used for the experiments and the fraction of η_{Heat} = 12.5% being again the only free (fitting) parameter results in a heat load of $Q_{1D} \cong 3 \cdot 10^4$ J/m^2. The feed rate of v = 6 m/min together with the laser spot diameter of d_{Beam} = 15 µm resulted in a local interaction time of $t_{IntAct}(6\ m/min) = d_{Beam} / v$ = 0.15 ms. For the lower feed rate of 0.12 m/min the interaction time was $t_{IntAct}(0.12\ m/min)$ = 7.5 ms. The resulting heat accumulation temperature increase $\Delta T_{HA,1D}$ of the calculation with the above numbers is shown in Fig. 7(a).

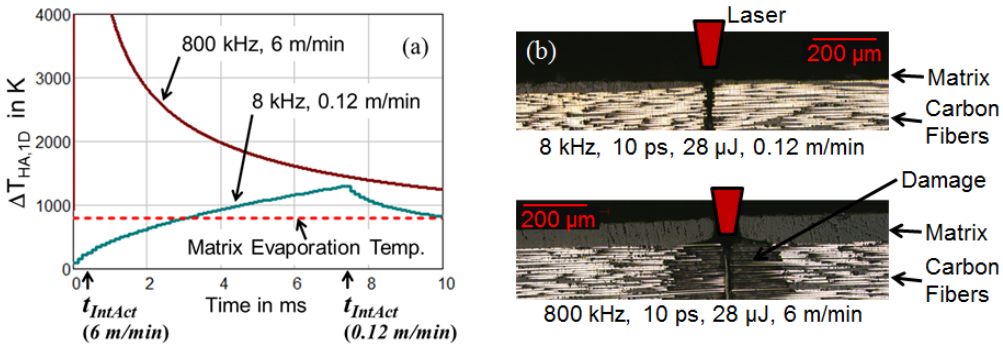

Fig. 7. Calculated temperature increase ΔT_{1D} for the carbon fibers in CFRP (a) and the resulting cross-sections when CFRP is experimentally processed with the corresponding parameters.

It is clearly seen that with a repetition rate of 800 kHz and a feed rate of v = 6 m/min (upper curve) very strong heat accumulation occurs during the interaction time of 0.15 ms with the laser beam. The temperature increase caused by heat accumulation significantly exceeds the matrix evaporation temperature of about 800 °C (dashed line) and even exceeds the evaporation temperature of Carbon of about 4000 K, which is however outside the validity of the model. If the feed is reduced by a factor of 50 and the repetition rate is reduced by a factor of 100 to 8 kHz (green line) the temperatures caused by heat accumulation remains below the evaporation temperature of the CFRP matrix for the hole interaction time of 7.5 ms.

The practical verification of this finding is illustrated by Fig. 7(b) with the depicted cross section of CFRP which was laser cut with the same parameters as used in the calculations.

#207073 - $15.00 USD Received 24 Feb 2014; revised 29 Mar 2014; accepted 31 Mar 2014; published 2 May 2014

The laser is incident from top. The first gray layer on top of the material is the plastic matrix cover. In the layer below the fibers are oriented parallel to the plane of the picture. One can see that with the low repetition rate and low feed rate (top picture) almost no damage occurs to the matrix material surrounding the carbon fibers. At the higher repetition rate of 800 kHz the thermal damage of the matrix extends up to about 200 µm in the surrounding material despite the higher feed rate which confirms the above interpretation of the calculations.

8. Maximum tolerable average power

The discussion so far indicates that the temperature increase, $\Delta T_{HA,nD}$, caused by heat accumulation should be limited to below a defined critical maximum temperature increase ΔT_{Max} to ensure given quality criteria. For metals this is usually the melting temperature. In view of the productivity of laser processing it is therefore of great interest to determine at what average power this critical temperature increase is reached. The sum in the heat accumulation Eq. (10) is of the form $\sum_{N=1}^{N_t} N^{-nD/2}$ which is the well-known harmonic series. Its value is shown in Fig. 8 for the three cases of $nD \in [1,2,3]$.

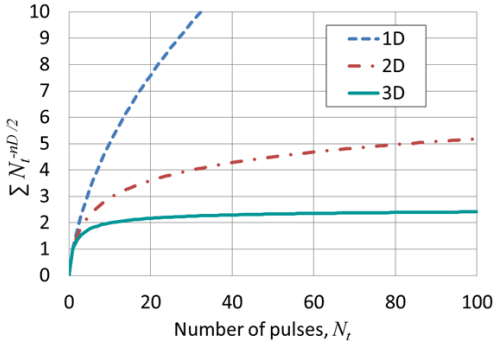

Fig. 8. Result of the Sum $\sum_{N=1}^{N_t} N^{-nD/2}$ for the three cases $nD \in [1,2,3]$ as a function of the number of pulses N_t.

For $N_t \to \infty$ the harmonic series converges if the exponent n/2 > 1. This means that for a large number of pulses on the same position the temperature increase on the surface caused by heat accumulation converges to a finite temperature in the case 3D heat flow while there is no temperature limit in the case of 1D and 2D heat flow.

In the most important 3D heat flow with a point source on the surface, the sum $\sum_{N=1}^{N_t} N^{-nD/2}$ converges to about 2.6 for $N_t \to \infty$ (solid green line in Fig. 8). Replacing the sum by this value in the heat accumulation Eq. (10) and using Eq. (4c) the condition to avoid a critical heat accumulation temperature increase reads

$$\Delta T_{Max} \geq \frac{2 \cdot Q_{Heat}}{\rho \cdot c_p \cdot \sqrt{\left(4 \cdot \pi \cdot \frac{\kappa}{f_L}\right)^3}} \cdot 2.6 \qquad (11)$$

or, with Eq. (2),

$$\Delta T_{Max} \geq \frac{5.2 \cdot \eta_{Heat}}{\rho \cdot c_p \cdot \sqrt{(4 \cdot \pi \cdot \kappa)^3}} \cdot \sqrt{f_L} \cdot f_L \cdot E_{Pulse} \qquad (12)$$

#207073 - $15.00 USD Received 24 Feb 2014; revised 29 Mar 2014; accepted 31 Mar 2014; published 2 May 2014

The product $f_L \cdot E_{Pulse} = P_L$ is the average laser power. Combining all material and geometrical constants into a figure of merit

$$c_{FOM} = \frac{\rho \cdot c_p \cdot \sqrt{(4 \cdot \pi \cdot \kappa)^3}}{5.2} \tag{13}$$

having the units $W / \left(\sqrt{s} K\right)$ and solving Eq. (12) for P_L one finds

$$P_L \leq \frac{\Delta T_{Max} \cdot c_{FOM}}{\sqrt{f_L} \cdot \eta_{Heat}} \tag{14}$$

This simple equation defines the maximum average power which is tolerable for a given repetition rate f_L at one single position to avoid that the heat accumulation increases the temperature by more than the critical temperature increase ΔT_{Max}. It is noted that in the 3D case discussed here the maximum tolerable average power is proportional to $f_L^{-1/2}$ and therefore decreases with increasing pulse repetition rate!

9. Implication on laser processing system design

Equation (14) gives a very useful guideline for the design of laser processing systems as described in [34]. As an example the maximum allowed average power for processing of CrNi-steel as shown in Fig. 1 is given in the following.

Setting ΔT_{Max} = 1500°C to be the melting temperature and using η_{Heat} = 12.5%, from the above drilling example the power limit for steel is given by $P_L < 3200 W / \sqrt{f_L / Hz}$. As discussed above, η_{Heat} strongly depends on the experimental conditions and might vary from close to 0% up to 100% if the intensity is below ablation threshold. In addition, the material parameters are usually not exactly known. Therefore η_{Heat} can be used as only free parameter in order to correctly describe the experimental results. For explaining the above CrNi-steel and CFRP experiments η_{Heat} had to be set to 12.5% ± 1%.

With a repetition rate of 10 kHz the maximum applicable average power for the CrNi-steel example therefore would be 32 W. Today, power scaling of ps-lasers is often realized by increasing the repetition rate. According to Eq. (14) this is very unfavorable. In fact, assuming a repetition rate of 1 MHz the maximum average power would be only 3.2 W!

Hence, following this thoughts, when using lasers with high repetition rates, one should ideally avoid to have more than one single pulse on the same spot by moving the beam fast enough. The minimum feed rate required for this is given by $v_F = d_F \cdot f_L$. For a repetition rate of 1 MHz and a focal spot diameter of 20 µm this results in a required feed rate of at least 20 m/s. It should be pointed out that reducing the laser spot size in order to reduce the required feed rate increases the intensity with a square dependence which might again result in reduced quality due to strong plasma formation.

10. Conclusion

Short-pulse laser processing has a large potential for very precise and low damage processing. However, the comprehensive treatment of multi-pulse processing presented in this paper reveals the basic mechanisms of heat accumulation and its consequence for the resulting quality. The formalism allows to estimate the maximum allowed average power for given repetition rates and for given materials.

Acknowledgments

This work was supported by the German Research Foundation (DFG) within the funding program Open Access Publishing.

#207073 - $15.00 USD Received 24 Feb 2014; revised 29 Mar 2014; accepted 31 Mar 2014; published 2 May 2014